Microcavity Array Supported Lipid Bilayer Models of Ganglioside - Influenza Hemagglutinin$_1$ Binding

Guilherme B. Berselli,[a1] Nirod Kumar Sarangi,[a1] Aurélien V. Gimenez,[a] Paul V. Murphy[b] and Tia E. Keyes*[a]

[a]School of Chemical Sciences and National Biophotonics and Imaging Platform, Dublin City University, Dublin 9, Ireland.

[b]School of Chemistry, NUI Galway University Road, Galway. Ireland.

*E-mail:tia.keyes@dcu.ie

The binding of influenza receptor (HA1) to membranes containing different glycosphingolipid receptors was investigated. We observed that HA1 preferentially binds to GD1a but the diffusion coefficient of the associated complex at lipid bilayer is approximately double that of the complexes formed by HA1 GM1 or GM3.

Supported lipid membrane models (SLBs) are important biophysical tools to understand protein-lipid/glycolipid interactions in controlled conditions.[1] Although highly stable, they typically exhibit reduced lipid lateral mobility, compared to liposomes, due to frictional substrate-membrane interactions.[2] Conversely, microcavity pore supported lipid membranes (MSLBs), offer liposome-like fluidity whilst maintaining much of the stability and versatility of SLBs, including the prospect of controlled asymmetric lipid leaflet composition inaccessible in liposomes.[3] MSLBs are therefore, particularly useful in the study of assembly processes at the lipid membrane that require lateral diffusion of constituent elements. This was exemplified recently in a study of cholera toxin (CTb)-GM1 recognition at asymmetric and symmetric MSLBs containing sphingomyelin and cholesterol.[4]

The influenza virus causes human respiratory illness and is responsible for seasonal and unpredictable pandemic infections.[5] To gain entry to the cytoplasm, influenza A viral protein hemagglutinin (HA) associates with sialylated receptors at the extracellular leaflet of the eukaryotic cell membrane.[6,7] Glycosphingolipids (GSLs) are an important group of hemagglutinin receptors comprised of hydrophobic ceramide backbone attached to oligosaccharide head groups.[8] Glycan microarrays have revolutionized understanding of HA glycan recognition.[9,10] However, artificial glycan arrays lack the cell membrane's fluidity which is intrinsic to the surface that HA encounters in-vivo.[11] There have been numerous investigations into the role of lipid membrane composition on influenza binding, at both cells and membrane models, including at supported lipid membrane models applied to HA_1-GSL binding.[12] For instance, the fusion of the H3N2 virions was demonstrated at SLBs comprised of PC/GM3 and H1N1 at liposomes comprised of PC/PE with GD1a as the

HA_1 receptor.[13,14] However, the role of the host cell membrane composition as well its fluidity in promoting or inhibiting influenza virus HA -glycan association has not been fully elucidated.[15–17] It has been shown, in liposomes, for example, that the transmembrane domain of HA partitions selectively to liquid ordered (L_o) domains, and in turn manifests clustering and budding of virus,a pathway for viral replication mediated potentially, by lipid rafts.[17–20].

Other factors such as acyl chain and sugar head composition, can affect GSL-protein recognition, and thus are likely to affect HA binding.[21] Simple models that can deconvolute the unit constituents of membrane composition in viral and eukaryotic membranes can yield insights into receptor recognition that may prove useful in both advancing fundamental insights and also as biomedically relevant platforms for understanding affinities of key components in infection for drug targets. Here, we combine electrochemical impedance spectroscopy (EIS) with Fluorescence Lifetime Correlation Spectroscopy (FLCS) to assess the relative affinity of HA_1 toward different GSLs within different membrane compositions at MSLBs. This study focuses on the monomeric globular head domain, HA_1, of influenza HA (noting in its native form it is a homotrimeric glycoprotein).[22] HA_1 contains the sialic acid receptor binding site responsible for cell membrane attachment and it is also an important epitope for neutralization antibodies against the influenza virus.[23] This analysis was carried out at the nanomolar concentration range of HA_1.

A 1 cm^2 gold electrode imprinted with an ordered array of uniform semi-spherical pores of 1 µm diameter were prepared by gold electrodeposition following the method previously described (detailed in SI).[24,25] To enhance bilayer stability, the exterior, top, surface of the arrays was selectively functionalized with a monolayer of 6-mercaptohexanol (SI). For FLCS studies, MSLBs were assembled at optically transparent, polydimethylsiloxane (PDMS) microcavity arrays as previously reported.[24,25] Lipid bilayer was assembled by depositing a lipid monolayer at pre-aqueous filled pore arrays by the Langmuir Blodgett deposition, followed by vesicle fusion of the proximal monolayer. This approach, reported previously, permits ready preparation of asymmetric bilayer compositions.[4] In nature, glycosphingolipids are isolated to the outer leaflet of the cell membrane, thus, we assembled the GSLs only at the distal leaflet of the MSLBs by incorporating them into the liposomes used for the vesicle fusion step (See Fig. S1, SI). Whereas EIS measurements are label-free, for FLCS, fluorescently labelled DOPE-ATTO655 (0.01 mol%) was mixed into the lipid bilayer and the influenza HA_1 was labelled with ATTO532 following the method described in Fig. S2, (SI).

We first evaluated the affinity of HA_1, using EIS, toward the individual GSLs; GM1, GM3 and GD1a, where each was doped at 1 mol% into model DOPC lipid bilayers (the most fluidic membrane) at gold-supported MSLBs. Figure 1a shows a representative Nyquist plot obtained from DOPC bilayer containing 1 mol % of GM1 at different concentrations of HA1. The relative Faradaic charge transfer resistance (R_{CT}) was obtained from the diameter of the semicircle of the Nyquist plot by fitting the experimental data to an equivalent circuit model (ECM) (inset, Fig.2a), a heuristic model reported earlier by us for suspended bilayer over microcavity pores.[4,24] Note that a constant phase element (CPE) was used instead of a pure capacitor to

obtain the best fit. The relative change to membrane resistivity (ΔR) after exposure to HA_1 was deduced from the initial membrane resistivity at 0 nM HA_1. As expected HA_1 binding increased membrane resistance, due to decreased admittance through the interfacial HA layer. This is also reflected in decreased membrane capacitance (ΔQ) values (cf. Fig. S3a, SI). Decreases to capacitance likely reflect increasing membrane thickness and may also reflect convolution of membrane thickness changes with changes to membrane roughness (or curvature), that impact the membrane area on HA association. The relative change in charge transfer resistance (ΔR) was plotted against HA_1 concentration (0 - 100 nM), Fig.1b (filled symbols). From Fig.1b it can be seen that by ~100 nM saturation binding is reached for each GSL. We fit the experimental ΔR data (dashed lines, Fig.2b) to the Hill-Waud binding model (SI) which applies to cooperative protein-receptor binding (Hill coefficient, n dependency, see SI).[26] From our fit, the empirical apparent equilibrium dissociation constant K_D values were estimated and indicate that HA_1 has highest affinity for GD1a (17.47±2 nM, n=2.56) followed by GM3 (23.96±4 nM, n=1.45) with lowest affinity recorded for GM1 (41.3±9 nM, n=1.81) at DOPC membranes (cf. Table S1, SI). These differences in affinity are not surprising given each GSLs differs in their oligosaccharide group constitution. GD1a is notably different in that it terminates with two sialic acid (n-acetylneuraminic acid) residues compared to one for GM1 and GM3. In addition, the packing of the GSLs in the lipid bilayer may play a role in affinity. GM1 and GM3 are known to pack differently in the membrane, e.g., ganglioside aggregation balances hydrogen bond interactions and steric hindrance of the headgroups, causing differences to clustering of GSLs depending on the headgroup involved.[27,28] The differences in packing are likely reflected in the very different magnitudes of ΔR response for the GSLs on HA binding.

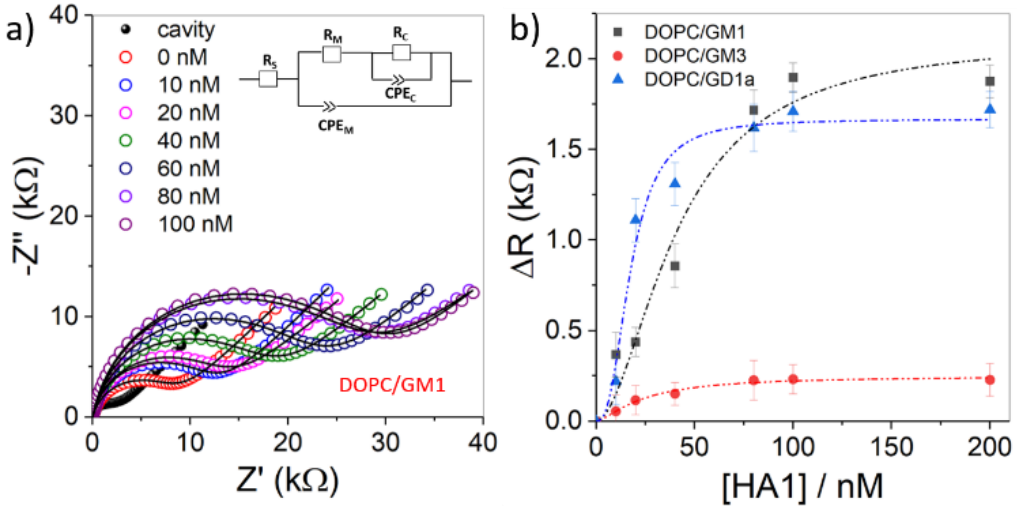

Figure 1. HA_1 binding to different GSLs in DOPC MSLBs formed in gold microcavities array. (a) Nyquist plot of cavity array before bilayer deposition (open black). EIS data of DOPC bilayer with GM1 (1 mol%) before HA_1 red and after HA_1 incubation (red: 0 nM, blue: 10 nM, pink: 20 nM, green: 40 nM, dark purple: 60 nM, light purple: 80 nM and violet: 100nM). Solid lines show the fit using ECM (inset). (b) Relative variation of the DOPC bilayer resistivity (ΔR) on HA_1 binding to bilayers containing 1 mol% of different glycolipids. The

dashed curves were fit to the Hill-Waud model. All the EIS spectra recorded in the presence of 1 mM $Fe(CN)_6^{3-/4-}$ and 0.1 M KCl at a bias potential of +0.26 V vs. Ag/AgCl (1 M KCl) with an amplitude 10 mV and frequency range of 10^4 to 10^{-2} Hz. All the measurements were carried out at 22±1 °C. The error bars in b, are ± SD, and the measurements are from triplicate.

Control experiments to evaluate non-specific binding in the absence of GSLs were carried out. And, as expected, no impedence changes were evident on incubation of HA_1 across any of the membranes explored in the absence of GSL. This observation was further confirmed from fluorescence data (Fig S4, SI).

Next, the interaction of HA_1 with each GSL at DOPC membrane was investigated using fluorescence lifetime correlation spectroscopy (FLCS) at PDMS-MSLB platform, to evaluate the lateral diffusivity of fluorescently labelled HA_1 (HA_1-ATTO532).

Figure 2 shows representative autocorrelation function (ACF) data obtained for HA_1-ATTO532 after incubation with an MSLB of DOPC/GM1 (1 mol%) (blue circles), DOPC/GD1a (1 mol%) (orange circles) and DOPC/GM3 (1 mol%) (green circles). Free HA_1 (in the absence of bilayer) HA_1-ATTO532 (red) and ATTO532 (black) dye in PBS solution.

The diffusion coefficients of ATTO532 (Fig.2, black circles) and labelled HA_1 (Fig.2, red circles) in PBS solution (pH 7.4) (each at 10 nM) were calculated by fitting the ACFs to a 3D model (See SI) as 385 $\mu m^2.s^{-1}$ and 90 $\mu m^2.s^{-1}$ respectively, which indicates a HA_1 hydrodynamic radius of approximately 2.4 nm. The lateral diffusion coefficient of HA_1-ATTO532 at GSL-containing MSLB was obtained by fitting the ACFs to a 2D diffusion model (See SI) and was determined as 13 $\mu m^2.s^{-1}$ for DOPC/GD1a and 5 $\mu m^2.s^{-1}$ for DOPC/GM1 and DOPC/GM3. The anomalous coefficient (α) value was obtained as ~1 in all cases, indicating Brownian diffusion.

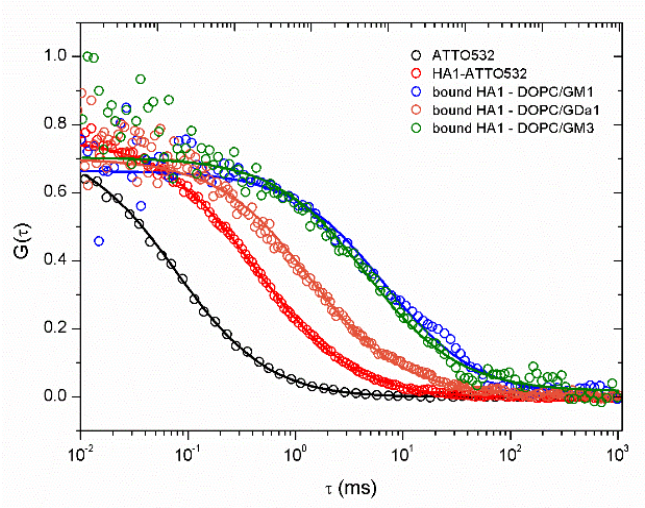

Figure 2 FLCS fitted autocorrelation functions (ACFs) obtained for free ATTO532 (black circles) and labelled HA_1-ATTO532 (red circles) in PBS (pH 7.4). After incubating labelled HA_1-ATTO532 to MSLBs comprised of

DOPC containing 1 mo%l of GM1 (blue circles), GM3 (green circles) and GD1a (orange circles). The bound fraction of HA1 was obtained by fitting the data to a one diffusing component model using 10 nM of dye/labelled protein.

The distinction in the lateral diffusion of HA_1 bound to GD1a and GM1 or GM3 is notable, given the ceramide tails of each glycolipid are analogous, the anticipated 1:1 binding would be expected to yield similar diffusion coefficients at a homogenous DOPC bilayer. The distinction indicates, interestingly, that the radius of the final membrane bound HA_1-GSL complex is different for GD1a compared to GM1 or GM3. The diffusion value was therefore used to estimate the diameter of membrane associated complex, from the Saffman-Delbrük (SD) model (SI). Using the SD model, we obtained a radius of 0.30 nm for GD1a, which corresponds well with that expected for diffusion of a single GD1a lipid. In contrast, a radius of 7.0 nm for the assembly formed by GM1/GM3 binding was estimated. As HA_1 is monomeric and presents a single binding site, the differences in size/diffusion value cannot be ascribed to multivalency. However, the distinctions may be attributed to variation in penetration of HA into the membrane as it accommodates the glycolipid binding, or may be due to self-association of glycolipids within the membrane. Although no evidence of lateral aggregation of HA_1 was observed even after prolonged incubation with GSL-containing membrane at saturation coverage of HA_1 as reflected in the homogeneity of the intensity-time traces (Fig. S5, SI). And, binding of HA_1-ATTO532 (10 nM, 40 nM or 80 nM, see Fig. S5, SI) at the membrane, was found not to influence membrane diffusivity significantly.

Other parameters such as physical properties of membrane and phase, which are affected by membrane composition can influence the lateral organisation of GSLs and their clustering. And there is significant evidence that ordered domains and rafts can promote HA-glycan binding.[29–31] Furthermore, the lateral organization of GSLs can be affected by the membrane composition in purely liquid disordered (L_d) membranes which may also influence affinity for HA_1.[27,32] We, therefore used the MSLBs to investigate the impact of the membrane composition and L_o and L_d phase-separated domains on HA_1 binding to GM1. The membrane diffusivity for each composition was assessed from the lateral mobility of DOPE-ATTO655 lipid tracer in the absence of protein, and the protein diffusivity was determined with HA_1-ATTO532 at bilayers of DOPC, POPC and DOPC/SM/Chol (4:4:2) (mol/mol/mol) doped with 1 mol% GM1 at the distal leaflet. In parallel, the effect of HA_1 association was evaluated using EIS at gold arrays. The Faradaic charge transfer resistance (R_{CT}) of the aforementioned membranes and their relative change on exposure to HA_1 interactions are shown in Fig.3. Interestingly, the binding constant, roughly estimated from ΔR at 50% saturation, is essentially unchanged by membrane composition. Whereas in contrast, the relative magnitude of membrane resistance change varies widely with composition on association with HA_1 (Fig. 3). ΔR is most pronounced for DOPC MSLB, compared with POPC, and HA_1 exerted least impact on the resistance of the

ternary DOPC/SM/Chol membrane. For instance, at a fixed concentration of HA_1 (100 nM), corresponding to saturation binding, the ΔR obtained for DOPC (ΔR_{DOPC} = 1.9 kΩ) shows respectively 2 and 10 fold greater resistivity change compared to POPC membranes (ΔR_{POPC} = 0.9 kΩ) and DOPC/SM/Chol (ΔR = 0.2 kΩ) membrane. This is attributed to the much tighter packing of cholesterol-containing membranes. The diffusivity data for labelled DOPE from FLCS (Table S2) in the absence of HA_1 and for bound labelled HA_1 are given in (Figure 4b, Table S2).

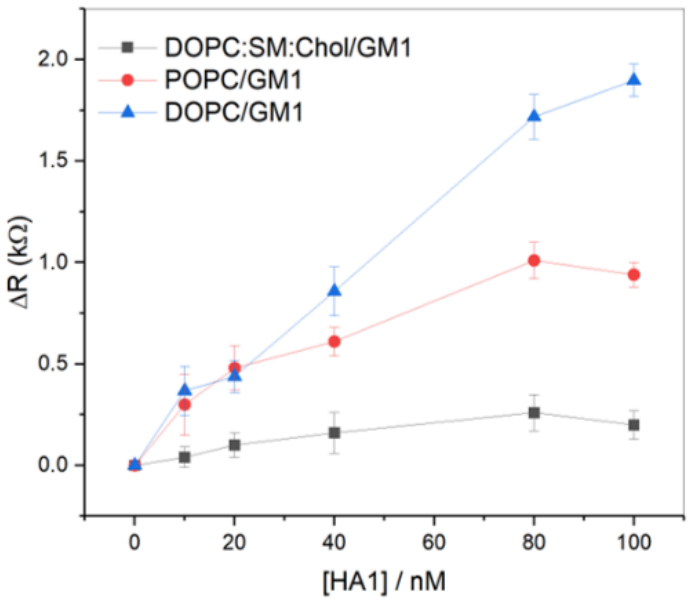

Figure 3 Representative resistance changes on HA_1 binding to GM1 (1mol%) at MSLBs of different lipid compositions. The addition of sphingomyelin and cholesterol reduces the clustering of Influenza receptor in comparison to the highly fluidic DOPC lipid bilayer. The asymmetric lipid bilayers are comprised of a DOPC layer (proximal leaflet) and DOPC/SM/Chol (4:4:2) (distal leaflet).

In the absence of HA_1, the lateral diffusion of labelled DOPE-ATTO655 was recorded as 10 $\mu m^2.s^{-1}$ for DOPC, consistent with previous reports,[3] 6.0 $\mu m^2.s^{-1}$ for POPC and 3.5 $\mu m^2.s^{-1}$ for DOPC/SM/Chol (4:4:2) membrane. The presence of 1 mol% GM1 at the distal leaflet did not affect measured fluidity. As expected, the data confirms membrane fluidity decreases in the order; DOPC > POPC > DOPC/SM/Chol (4:4:2), attributed in the latter case to mixed domain formation.[33] Within experimental error, the diffusivity of the lipid marker did not change upon HA_1-ATTO532 (10 nM) incubation irrespective of membrane composition. For the ternary DOPC/SM/Chol (4:4:2) composition, the diffusivity of the ordered lipid regions was obtained separately by measuring the lateral diffusion of labelled sphingomyelin (SM-ATTO647n), as 2.5 $\mu m^2.s^{-1}$, which is 3.5-fold lower than its diffusivity in DOPC membranes, 8.8 $\mu m^2.s^{-1}$ (Fig. S6, SI).

The lateral diffusion of membrane bound HA_1-ATTO532 is influenced profoundly by membrane composition and found to be 5.0 $\mu m^2.s^{-1}$ for DOPC, 3.3 $\mu m^2.s^{-1}$ for POPC and 1.6 $\mu m^2.s^{-1}$ for ternary lipid bilayers.

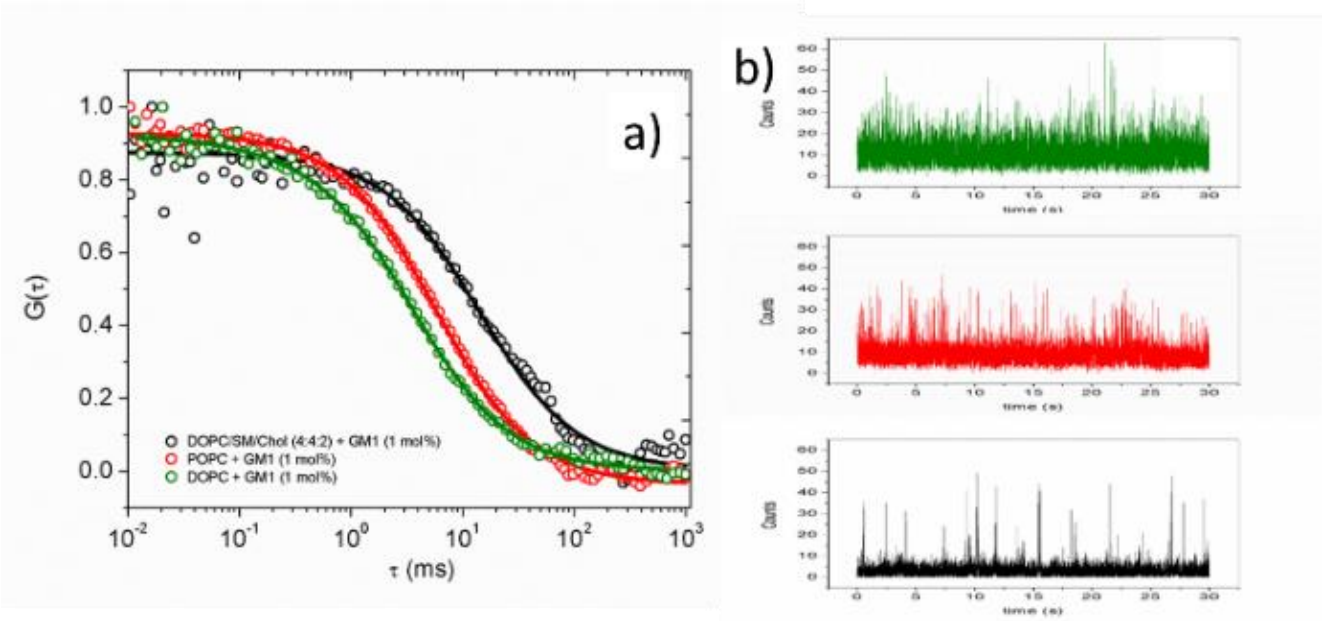

Figure 4 – a) Normalized autocorrelation function of HA_1-ATTO532 obtained from MSLBs of DOPC (green), POPC (red) and DOPC/SM/Chol (black). All lipid bilayers contain GM1 (1 mol%) in the distal lipid leaflet. (b) Illustrates corresponding fluorescence intensity time trace of labelled HA_1 at designated bilayer composition.

Notably, for DOPC and POPC the diffusion coefficient is roughly half that of the lipid label. Whereas for the ternary composition, the diffusion rate is lower than half, which suggests an association with ordered domains, consistent with previous report.[34] The number of labelled HA_1 molecules in the confocal volume may indicate that HA_1 has a higher preference to bind to GM1 in more fluidic membranes but based on EIS data the difference is not dramatic (Figure 4b, Table S2). It is worth mentioning that the curvature, as well as thermal fluctuation of membrane lipid, may affect the diffusivity of proteins, as observed in a previous study.[35]

Our results from EIS as well as FLCS revealed that HA_1 has an important predilection for binding GSLs in more fluidic membranes.

In summary, the affinity of three prevalent glycosphingolipids for influenza subunit HA_1 were compared. GD1a showed highest affinity at DOPC bilayers, but diffusivity of the resulting GSL-HA_1 complex was roughly half of that GM1 and GM3- HA_1 complexes indicating surprising differences in the assembly dimensions or associated HA_1 penetration into the lipid bilayer. The affinity of HA_1 for GM1 appears unaffected by bilayer composition. But the lower mobility of bound HA_1 in SM/Chol membranes suggests association with Lo domains. Overall, the data demonstrates that MSLBs are versatile platform for modelling unit steps in viral-

membrane interactions. These studies will next be extended to multivalent HA subtypes and related viral models.

The authors gratefully acknowledge Science Foundation Ireland under Grant No. [14/IA/2488]

Conflicts of interest

There are no conflicts to declare.

[1] These authors contributed equally.

Notes and references

1 I. Carton, Lucy Malinina and R. P. Richter, *Biophys J*, 2010, **99**, 2947–2956.

2 C. G. Siontorou, G.-P. Nikoleli, D. P. Nikolelis and S. K. Karapetis, *Membranes*, 2017, **7**, 38.

3 H. Basit, V. Gaul, S. Maher, R. J. Forster and T. E. Keyes, *The Analyst*, 2015, **140**, 3012–3018.

4 G. B. Berselli, N. K. Sarangi, S. Ramadurai, P. V. Murphy and T. E. Keyes, *ACS Appl. Bio Mater.*, 2019, **2**, 3404–3417.

5 J. K. Taubenberger and D. M. Morens, *Annu Rev Pathol*, 2008, **3**, 499–522.

6 D. A. Steinhauer, *Virology*, 1999, **258**, 1–20.

7 S. J. Gamblin and J. J. Skehel, *Journal of Biological Chemistry*, 2010, **285**, 28403–28409.

8 S. Degroote, J. Wolthoorn and G. van Meer, *Seminars in Cell & Developmental Biology*, 2004, **15**, 375–387.

9 J. Stevens, O. Blixt, J. C. Paulson and I. A. Wilson, *Nature Reviews Microbiology*, 2006, **4**, 857–864.

10 M. L. Huang, M. Cohen, C. J. Fisher, R. T. Schooley, P. Gagneux and K. Godula, *Chem. Commun.*, 2015, **51**, 5326–5329.

11 Y. Ji, Y. J. White, J. A. Hadden, O. C. Grant and R. J. Woods, *Curr Opin Struct Biol*, 2017, **44**, 219–231.

12 M. Müller, D. Lauster, H. H. K. Wildenauer, A. Herrmann and S. Block, *Nano Lett.*, 2019, **19**, 1875–1882.

13 J. Ramalho-Santos and M. C. Pedroso De Lima, *Cell. Mol. Biol. Lett.*, 2004, **9**, 337–351.

14 C. Godefroy, S. Dahmane, P. Dosset, O. Adam, M.-C. Nicolai, F. Ronzon and P.-E. Milhiet, *Langmuir*, 2014, **30**, 11394–11400.

15 R. Leiva, M. Barniol-Xicota, S. Codony, T. Ginex, E. Vanderlinden, M. Montes, M. Caffrey, F. J. Luque, L. Naesens and S. Vázquez, *J. Med. Chem.*, 2018, **61**, 98–118.

16 X. Sun and G. R. Whittaker, *Journal of Virology*, 2003, **77**, 12543.

17 P. Scheiffele, A. Rietveld, T. Wilk and K. Simons, *J. Biol. Chem.*, 1999, **274**, 2038–2044.

18 S. Scolari, S. Engel, N. Krebs, A. P. Plazzo, R. F. M. D. Almeida, M. Prieto, M. Veit and A. Herrmann, *J. Biol. Chem.*, 2009, **284**, 15708–15716.

19 M. Veit and B. Thaa, *Adv Virol*, 2011, **2011**, 370606.

20 M. Takeda, G. P. Leser, C. J. Russell and R. A. Lamb, *PNAS*, 2003, **100**, 14610–14617.

21 L. Malinina, M. L. Malakhova, A. T. Kanack, M. Lu, R. Abagyan, R. E. Brown and D. J. Patel, *PLoS Biol*, 2005, **4**, 1996–2011.

22 S. Jegaskanda, P. C. Reading and S. J. Kent, *The Journal of Immunology*, 2014, **193**, 469–475.

23 C.-C. Lee, C.-Y. Yang, L.-L. Lin, T.-P. Ko, A. H.-L. Chang, S. S.-C. Chang and A. H.-J. Wang, *Scientific Reports*, 2019, **9**, 1–11.

24 S. Maher, H. Basit, R. J. Forster and T. E. Keyes, *Bioelectrochemistry*, 2016, **112**, 16–23.

25 B. Jose, C. T. Mallon, R. J. Forster, C. Blackledge and T. E. Keyes, *Chem. Commun.*, 2011, **47**, 12530–12532.

26 J. Shi, T. Yang, S. Kataoka, Y. Zhang, A. J. Diaz and P. S. Cremer, *J Am Chem Soc*, 2007, **129**, 5954–5961.

27 R.-X. Gu, H. I. Ingólfsson, A. H. de Vries, S. J. Marrink and D. P. Tieleman, *J. Phys. Chem. B*, 2017, **121**, 3262–3275.

28 D. W. Lee, H.-L. Hsu, K. B. Bacon and S. Daniel, *PLOS ONE*, 2016, **11**, e0163437.

29 R. L. Wilson, J. F. Frisz, H. A. Klitzing, J. Zimmerberg, P. K. Weber and M. L. Kraft, *Biophysical Journal*, 2015, **108**, 1652–1659.

30 J. Nikolaus, S. Scolari, E. Bayraktarov, N. Jungnick, S. Engel, A. P. Plazzo, M. Stöckl, R. Volkmer, M. Veit and A. Herrmann, *Biophys J*, 2010, **99**, 489–498.

31 I. N. Goronzy, R. J. Rawle, S. G. Boxer and P. M. Kasson, *Chem. Sci.*, 2018, **9**, 2340–2347.

32 N. Fricke and R. Dimova, *Biophys. J.*, 2016, **111**, 1935–1945.

33 D. Marsh, *Biochimica et Biophysica Acta (BBA) - Biomembranes*, 2009, **1788**, 2114–2123.

34 D. V. Nicolau, K. Burrage, R. G. Parton and J. F. Hancock, *Mol Cell Biol*, 2006, **26**, 313–323.

35 E. Reister and U. Seifert, *Europhys. Lett.*, 2005, **71**, 859–865.